International Journal of Heat and Mass Transfer 51 (2008) 6259–6267

Contents lists available at ScienceDirect

International Journal of Heat and Mass Transfer

journal homepage: www.elsevier.com/locate/ijhmt

An experimental study on the thermal conductivity of aluminium foams by using the transient plane source method

E. Solórzano [a], J.A. Reglero [a], M.A. Rodríguez-Pérez [a,*], D. Lehmhus [b], M. Wichmann [b], J.A. de Saja [a]

[a] Cellular Materials Group (CELLMAT), Condensed Matter Physics Department, Faculty of Science, University of Valladolid, 47011 Valladolid, Spain
[b] Fraunhofer Institute for Manufacturing Technology and Applied Materials Research (IFAM), Wiener Strasse 12, 28359 Bremen, Germany

ARTICLE INFO

Article history:
Received 5 February 2007
Available online 17 June 2008

Keywords:
Aluminium foams
Thermal conductivity
Transient plane source method

ABSTRACT

The thermal conductivity of a collection of AlSi7 foams with porosities between 0.5 and 0.8 produced throughout the powder metallurgical route has been determined using the transient plane source technique (TPS). Several measurements have been performed on different surfaces of the foam blocks. The values obtained have shown an increase of effective thermal conductivity with density and a significant dependency with the zone of the foam where the experiments were performed. The results obtained have been explained in terms of local density trough images obtained from computed tomography, showing that the TPS technique is sensitive to in-homogeneities derived from the foaming process. Finally, several theoretical models for thermal conductivity have been unified, after suitable simplifications for this kind of materials, and have been compared with the experimental results.

1. Introduction

Cellular metals combine the advantages of a metal (strong, hard, tough, conductive both electrically and thermally, etc.) with the functional properties of a foam (lightweight, stiff and adjustable density and/or cellular structure). Because of this, metal foams are interesting in a number of engineering applications such as structural panels, energy absorption devices, acoustic damping panels, compact heat exchangers, etc. [1]. Particularly, the thermal transport properties of metal foams are specially attractive in a wide variety of applications [2,3], such as thermal insulation, heat transfer etc., and are also important for the later processing of the metal matrix, e.g. in terms of thermal treatments.

Several investigations have dealt with this topic in the last years: Calmidi et al. and Bhattacharya et al. [4,5] studied the thermal conductivity of high-porosity fibrous foams ($V_g > 0.9$), showing an increase of the conductivity values with sample density. Boomsma and Poulikakos [6] investigated the influence of different fillers on the thermal conductivity of high-porosity foams. Babcsán et al. [7] measured the thermal conductivity of closed-cell aluminium foams at different temperatures using a steady state method. Abramenko et al. [8] determined the thermal conductivity of some closed-cell aluminium foams with porosity between 0.7 and 0.8, using a stationary method. Lu and Chen, in a theoretical paper, suggested that heat transfer is mainly due to solid conduction through faces and cell edges, neglecting radiation or convection even at high temperatures (500 °C) [9]. Lu et al. [10] investigated the heat transfer in open-cell foams. Paek et al. [11] studied the influence of cell size in the thermal conductivity of open-cell aluminium foams with porosities in the range of 0.85 and 0.9. Convection and forced convection mechanisms have been treated from the experimental and theoretical point of view [12–14] by several authors. Moreover, excellent revisions of theoretical–analytical models related to heat conduction in cellular materials have been written by Collishaw and Leach [15,16]. The topic of thermal conductivity in cellular materials can also be approached by numerical methods such as finite element [17,18] or Monte–Carlo [19] methods as found in the literature.

Most of these papers are focused on open-cell foams, and only two of them deal with closed-cell metal foams, in all cases foams of high or medium–high porosity. In general terms, there is a lack of experimental data related to closed-cell foams with lower porosities and experimental results of the thermal conductivity of the bulk foam, i.e. with the outer skin present in the measurement direction. In the present work, we have used the transient plane source technique (TPS) to measure the thermal conductivity of several closed-cell aluminium foams with porosities between 0.5 and 0.8.

From the previously cited papers, it is well know that thermal conductivity of cellular materials is very sensitive to density. Therefore, it should be expected that this property could also be sensitive to density gradients within a given sample. Since the TPS method allows measuring local or bulk thermal conductivity, this technique could become an alternative method to detect in-homogeneities in foam parts by measuring the thermal conductivity locally.

* Corresponding author. Tel.: +34 983184035; fax: +34 983423192.
E-mail address: marrod@fmc.uva.es (M.A. Rodríguez-Pérez).

0017-9310/$ - see front matter © 2008 Elsevier Ltd. All rights reserved.
doi:10.1016/j.ijheatmasstransfer.2007.11.062

List of symbols

$R(t)$	hot-disk sensor resistance (Ω)
R_0	hot-disk sensor initial resistance (Ω)
T	temperature (K)
α	temperature coefficient of resistance (Ω/K)
τ	relation between measurement time and characteristic time
θ	characteristic time (s)
a	sensor radius (m)
κ	thermal diffusivity (m^2/s)
λ_{gs}	thermal conductivity due to gas and solid phases (W/m K)
λ_s	thermal conductivity of solid phase (W/m K)
λ_g	thermal conductivity of gas phase (W/m K)
V_g	porosity of the foam ($0 < V_g < 1$)
ρ_f	density of the foam (kg/m^3)
ρ_s	density of the solid material (kg/m^3)
ξ	efficiency factor in Ashby model
f_s	mass fraction in the cell edges in a cellular material ($0 < f_s < 1$)

In recent years considerable advances in traditional manufacturing processes for aluminium foams have been reached and a high number of new manufacturing methods have been developed obtaining a high homogeneity in terms of density and cellular structure [20,21]. However, the stochastical nature of the production processes may still cause defects and in-homogeneities in the cellular structure, such as big pores, a non-uniform thickness of the outer skin and defects in the cellular structure. Some investigations [22–24] have been performed to this end, exploring with different non-destructive techniques (micro-computed tomography, ultra small-angle neutron scattering, etc.) the internal structure of the foam. Nevertheless, these non-destructive methods are difficult to implement in an industrial production line because of the cost and the long time needed to obtain the data.

Bearing all these previous ideas in mind, the present paper has two main objectives: firstly, to measure thermal conductivity of a collection of closed-cell AlSi7 foams with porosities between 0.5 and 0.8 using the TPS method, and to analyse the results by comparing them to predictions gained from the most common theoretical models both of analytical and empirical type. Secondly, to evaluate the ability of the TPS method to detect in-homogeneities in a given metal foam, and thus evaluate its suitability and its limitations as a tool for quality control. For this purpose, computed tomography (CT) technique was employed as an auxiliary technique to study the internal density distribution of the samples and correlate it with the thermal conductivity values obtained.

2. The TPS method

2.1. An introduction to the TPS method

Measurement of thermal conductivity by means of the TPS method has been demonstrated elsewhere [25,26]. The basic principle of this method relies on a plane element which acts both as temperature sensor and heat source. This element consists of an electrically conducting pattern of thin nickel foil (10 μm) spiral-shaped, embedded in an insulating layer usually made of Kapton (70 μm thick). The TPS element is located between two samples with both sensor faces in contact with the two samples surfaces as Fig. 1 depicts. Two samples of similar characteristics are required for this purpose.

This method offers some advantages in comparison with standard methods, such as fast and easy experiments, a wide range of thermal conductivities accessible (from 0.02 to 400 W/m K), marginal effort needed in sample preparation, flexibility in sample size and a possibility to perform local or bulk measurements with only changing the sensor diameter. It is important to remark that this is a contact method, so special care is needed in the experimental procedure (Section 2.3).

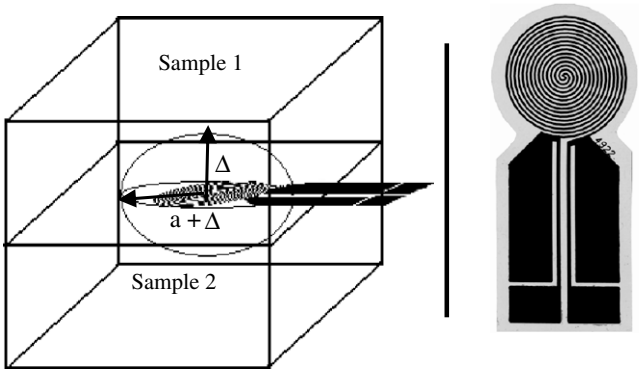

Fig. 1. Experimental set-up to perform TPS measurements and sensor shape.

2.2. The TPS theory

A constant electric power supplied to the sensor results in an increase in temperature $\Delta T(t)$ which is directly related to the variation in the sensor resistance $R(t)$ by the equation:

$$R(t) = R_0[1 + \alpha \Delta T(t)] \quad (1)$$

where R_0 is the nickel electrical resistance in the beginning of the recording (initial resistance), α is the temperature coefficient of resistance of the nickel foil, and $\Delta T(t)$ is the temperature increase of the sensor with time.

Assuming an infinite sample and the conductive pattern being in the XY plane of a coordinate system, the temperature rise at a point (XY) at time t is obtained by solving the equation for the heat conduction, which relates change in temperature with time [27]. In the particular case of our sensor geometry, n concentric ring sources, the spatial average $\overline{\Delta T(\tau)}$ can be obtained through the equation [25,26]:

$$\overline{\Delta T(\tau)} = P_0(\pi^{3/2} a \cdot \lambda)^{-1} D(\tau) \quad (2)$$

where P_0 is a Bessel function, $D(\tau)$ is a geometric function characteristic of the number "n" of concentric rings, and $\overline{\Delta T(\tau)}$ is the temperature increase of the sensor expressed in terms of only one variable τ, defined as

$$\tau = (t/\theta)^{1/2}; \quad \theta = a^2/\kappa \quad (3)$$

where t(s) is the measurement time from the start of the transient heating, θ is the characteristic time, which depends both on parameters of the sensor and the sample, a(mm) is the sensor radius and k(mm^2/s) is the thermal diffusivity of the sample. The characteristic time needs to be in the range 0.5–1.5 to guarantee that the theoretical assumptions are kept, thus the heat flow is an ellipsoid of neither too high nor too low sphericity.

Thermal conductivity can be obtained by fitting the experimental data to the straight line given by Eq. (2); thermal diffusivity is calculated from Eq. (3) taking into account the τ value determined in the previous fit.

For these experiments, one of the most important parameter is named *probing depth* (Δ). This parameter gives the distance that the heat flow reaches into the material from any point of the disk surface (Section 5.1).

2.3. Experimental procedure

As TPS is a contact method, a special care has to be taken to minimize thermal contact resistance. The good heat transition trough two different materials is mainly associated to contact pressure and surface roughness [28,29]. These parameters were kept constant in our experiments. A constant force of 20 N was applied. Additionally, the foams outward skin was polished in order to reduce the thermal contact resistance.

Moreover, the TPS equipment is able to compensate the heat capacity of the sensor and other thermal delays of the heat flow by introducing a time correction. Nevertheless, it is necessary to suppress the first 20–30 points of each measurement (of a total of 200 points of the heating curve) to eliminate the heat capacity of the sensor that cannot be fully compensated by the time correction [25–27].

Finally, to avoid residual temperature drifts on the samples, it was necessary to fix a time span of 20 min between individual experiments on each specimen.

3. Materials

In the course of this study, aluminium foam samples containing 7 wt.% Si have been produced by the powder metallurgical (PM) or Fraunhofer route [20]. Silicon supplied by Ölschläger was added as elementary powder to Al99.7 powder of grade AS71 supplied by ECKA Granules. No further alloying elements were used. For all the foamable precursor materials studied, 0.5 wt.% titanium hydride powder of Chemetall's grade N was chosen as a blowing agent. Consolidation to a foamable precursor material was reached by means of cold isostatic pressing and subsequent hot extrusion.

To produce foam specimens, a suitable piece of the foamable precursor material was inserted into a cuboid steel mould. Dimensions of the mould were 200 mm length, 65 mm width and 65 mm height. Foaming was carried out in a batch furnace at temperatures between 630 °C and 750 °C. Different foaming temperatures and exposure times were tested, producing different densities. Each foam of dimensions as given above was cut in three individual samples, namely a, b and c, dimensions of which were $60 \times 65 \times 65$ mm^3. Fig. 2 illustrates the way these specimens were cut from the foam originally produced. Furthermore, Fig. 2 shows how the directions of measurement used in the determination of thermal conductivity values relate to the geometry of the original foam body and to the principal direction of expansion. Table 1 shows the average density of the samples under study, which varied between 520 kg/m^3 and 1350 kg/m^3.

After cutting of the foam blocks some clear in-homogeneities were appreciated in two foam blocks, namely block 1 and 5. Specifically, the most severe in-homogeneities were found in the block 5, specimens 5-a and 5-c, consisting of denser bottom faces and some big pores. On the other hand, high-density foams (blocks 6, 7 and 8) could all be considered homogeneous based on visual inspection and blocks 2, 3 and 4 seemed to be also homogeneous. Regarding high-porosity foams, a special remark deserves block 2 because of its low-density combined with a high homogeneity in pore size.

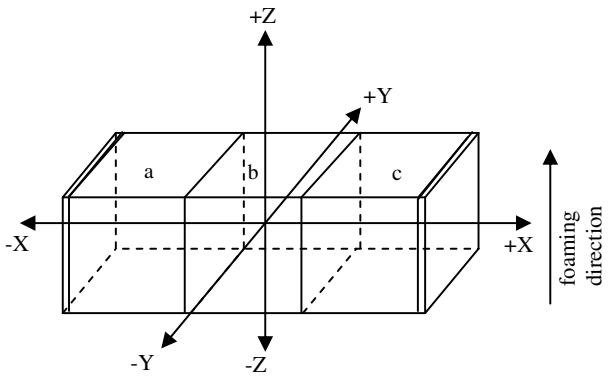

Fig. 2. Schematic drawing of the original foam block with the cuts performed and the reference directions.

Table 1
Nomenclature and density of the samples

Label	Density (g/cm^3)	Label	Density (g/cm^3)
1-a	0.53	5-a	0.87
1-b	0.53	5-b	0.75
1-c	0.52	5-c	0.83
2-a	0.55	6-a	0.93
2-b	0.63	6-b	0.93
2-c	0.58	6-c	0.91
3-a	0.70	7-a	0.95
3-b	0.63	7-b	1.05
3-c	Not available	7-c	1.00
4-a	0.73	8-a	1.27
4-b	0.78	8-b	1.35
4-c	0.77	8-c	1.33

In order to analyse the possible influence of local density on thermal properties some representative homogeneous specimens, namely 2-a and 2-b, and other non-homogeneous samples, in particular 5-a and 5-c, were chosen to be inspected by helical CT in a medical scanner.

4. Characterization of the cellular structure and microstructure

A quantitative evaluation of density distribution and a qualitative study of the cellular structure were performed by helical CT. The metal matrix microstructure was inspected by optical microscopy.

An helical medical scanner, mod. Siemens Somaton operated with software VA40C was used to examine the internal structure and the density distribution for the samples 2-a, 2-c, 5-a and 5-c. Fig. 3 shows some of the tomographies obtained for these samples. Although the scanner resolution is not high enough for a quantitative analysis of the cellular structure some interesting facts can be appreciated. Samples 5 are clearly in-homogeneous, a thick skin of aluminium is observed at the bottom surface, probably due to the drainage process. Moreover, a big pore can be observed close to the $-Y$ face, probably due to the coarsening mechanism or to cell-wall rupture during foaming. In contrast, samples 2 presented a more homogeneous structure, especially in case of sample 2-b.

Regarding density distribution, the density profiles for the three directions were calculated and are shown in Fig. 4. The X direction, i.e. perpendicular to the cut faces planes, is near to be homogeneous with an almost constant density profile, whereas the density along Y and Z axis changes from the nearly solid aluminium value, next to the outer skins, to very low densities in the middle part of the foam. It is also important to note that the density profile along

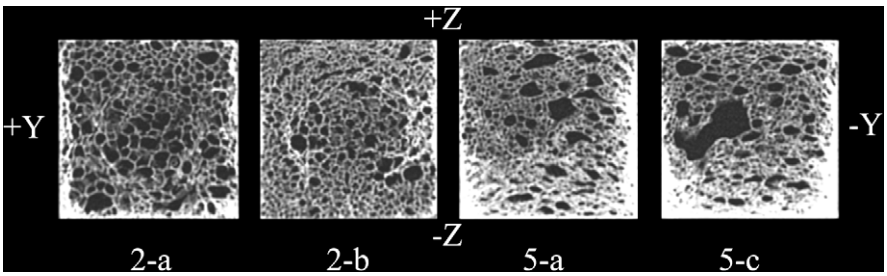

Fig. 3. Computed tomography images of samples for the in-homogeneity study.

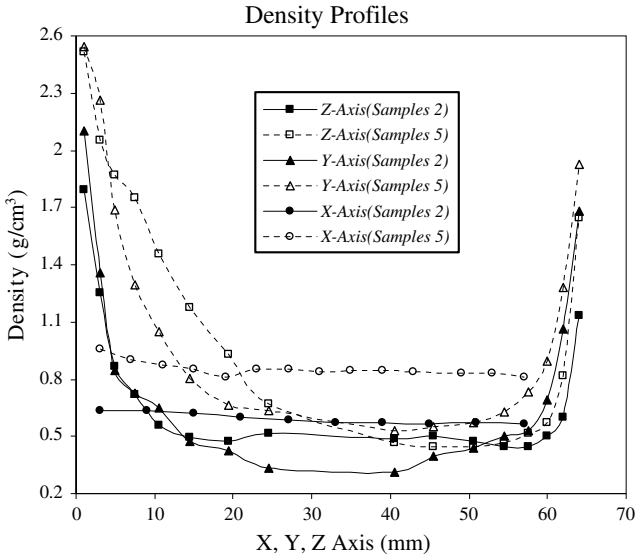

Fig. 4. Density profiles for *X*, *Y* and *Z* axes in samples 2 and 5.

Z axis for sample 5 is asymmetric, with a much denser bottom face showing higher density values up to 20 mm from the bottom part.

Since foaming temperatures and times differed among samples, which could affect metal matrix microstructure, a qualitative evaluation by optical microscopy was performed. The optical micrographs were taken in a Leica petrographic microscope mod. DMLP, equipped with a Leica digital camera mod. DC100. Results showed that the complete melting of the powder compact and the formation of the correspondent alloy, which in this case means the development of the characteristic Al–Si eutectic structure surrounding primary aluminium grain, occurred in all samples.

Fig. 5 shows the microstructure of three selected samples of different densities and different processing parameters. No obvious differences in grain size are observed, and variation in microstructure is limited to a slightly finer eutectic in the lowest density sample. Specifically, clear evidence for remaining Si particles originating from the Si powder, which would have indicated incomplete alloy formation, could neither be traced in the high nor in the low-density samples. Therefore, it can be assumed that the metal matrix had very similar thermal properties over the whole range of densities represented by the samples considered.

5. Results of thermal conductivity

Two different kinds of measurements have been carried out. The first characterization was done with the sensor in contact with the cut face, i.e. the face where the outer skin is not present (faces $-X$ and $+X$). Moreover a study of in-homogeneity was performed for the four faces with outer skin ($-Y$, $+Y$, $-Z$, $+Z$) on selected samples to compare these results with those for cut faces and with the density profiles for *Y* and *Z* directions.

5.1. Measurements in X direction

For this study the TPS sensor was located between two similar samples, as shown in Fig. 1. Output power was fixed at 0.4 W during the experiments and sensor radius was 9.7 mm. Measurement time was varied between 18 and 40 s to take into account the different thermal properties of each foam and to ascertain that a similar volume of foam was covered by the heat flow in foams of different density and thus different conductivity. This volume is represented by the probing depth parameter Δ, which is related to thermal diffusivity and time through the equation:

$$\Delta = \beta\sqrt{\kappa t} \tag{4}$$

with β an experimental factor near to 2 (κ is measured during each recording as was explained in Section 2.1).

It was necessary to modify measurement time as $t \propto \kappa^{-1}$ to obtain a nearly constant probing depth. It is important to remark that time variation is limited because it is necessary to assure that characteristic time is in the range from 0.5 to 1.5. In addition, this parameter Δ must be lower than the minimum distance between

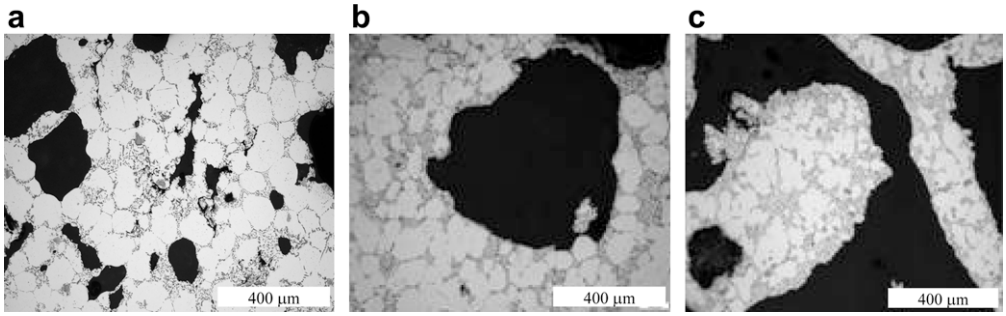

Fig. 5. Micrographs of some of the samples. (a) Sample 2a, (b) sample 5a and (c) sample 8a.

the sensor and the limit of the sample, to avoid that the heat flow reaches out of the sample. In our experiments this distance was about 25 mm; probing depth was approximately 19 mm for all the experiments. For this probing depth value we can consider we are performing a bulk measurement, because this value of 19 mm is next to half the size of the whole sample.

To perform the experiments, the samples of each block were studied in couples, namely a–b, a–c and b–c. Each couple of samples was measured in four different configurations, combining the cut faces in the experiments, carrying out five measurements in each configuration, to minimize experimental errors.

Table 2 presents the results obtained for each couple of samples, representing the average and the standard deviation in the four different configurations as a function of the averaged density of the two samples involved in each experiment.

The experimental data are plotted in Fig. 6 compared to the experimental values obtained by other researchers [4,5,7,8,11]. The effective thermal conductivity has been normalized according to the cited solid conductivity and a value of $\lambda_{AlSi7} = 167$ W/m K has been used to normalized our results [30]. Results for open and closed-cell foams are shown in the graph. As can be seen this work is verified by the results of other authors with the exception of the results obtained by Abramenko et al. which are out of the expected range according to the other research works. It is clear that the thermal conductivity values decrease non-linearly with sample porosity. On the other hand, due to the different characterisation methods, base alloys and cellular structures involved it is not recommendable to fit all the results together and thus only the results obtained in this paper are analysed in this work.

Regarding the possible effect of the density distribution on the measurements along *X* direction, Fig. 4 indicates there that are no appreciable differences in density along this axis for the samples 2 and 5 – these samples are two examples of homogeneity/in-homogeneity – so it is reasonable to consider that samples blocks from 1 to 8 are almost homogeneous in the *X* direction. Moreover, the high probing depths used in these experiments guarantees this homogeneity at least with respect to thermal conductivity values.

Table 2
Experimental values of thermal conductivity of AlSi7 foam samples

Samples	Average density (g/cm^3)	Average porosity	Thermal conductivity (W/m K)	Standard deviation (%)
1a–1b	0.53	0.80	14.3	3.40
1a–1c	0.52	0.81	14.9	1.14
1b–1c	0.52	0.81	14.6	0.88
2a–2b	0.59	0.78	20.2	1.70
2a–2c	0.56	0.79	16.4	2.77
2b–2c	0.60	0.78	20.8	3.30
3a–3b	0.68	0.75	20.9	3.37
4a–4b	0.75	0.72	21.4	1.47
4a–4c	0.75	0.72	20.0	1.38
4b–4c	0.77	0.71	23.6	2.46
5a–5b	0.81	0.70	29.4	7.64
5a–5c	0.85	0.68	28.2	3.82
5b–5c	0.79	0.71	23.9	1.85
6a–6b	0.93	0.65	27.8	4.88
6a–6c	0.92	0.66	31.3	6.92
6b–6c	0.92	0.66	30.1	1.47
7a–7b	1.00	0.63	30.7	3.26
7a–7c	0.97	0.64	33.9	2.60
7b–7c	1.02	0.62	36.5	2.97
8a–8b	1.33	0.50	51.6	6.65
8a–8c	1.30	0.51	62.2	4.99
8b–8c	1.34	0.50	65.0	7.23

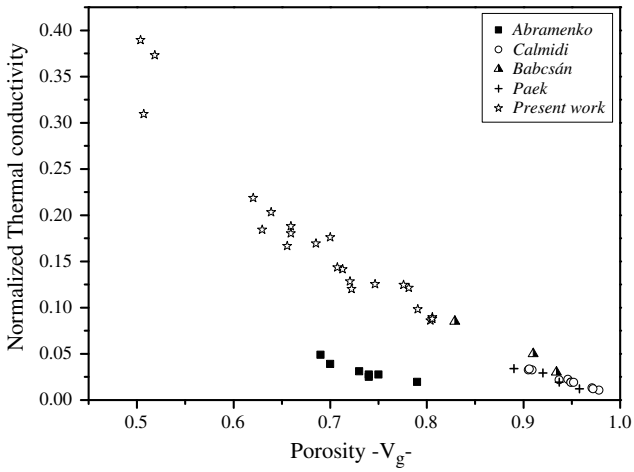

Fig. 6. Experimental results as function of density with included error bars.

5.2. Measurements in Y and Z directions (in-homogeneities detection)

In order to relate the presence of in-homogeneities to thermal conductivity several measurements were performed in different directions on the outer skin of the foams. As was previously explained in Section 2.1, by changing the disk radius it is possible to modify the probing depth. For these experiments we chose a smaller disk with a radius of 6.4 mm; the tests were performed with an average probing depth of 10 mm. Therefore, the sample volume covered by the heat flow had a higher density (Fig. 4). Obviously, the higher local density will affect values of thermal conductivity obtained with this sensor radius, which are thus not comparable to those obtained in the previous characterization.

To carry out this characterization samples 2-a, b and samples 5-a, c were tested with their common faces patterned. The thermal conductivity values obtained for both samples are presented in Table 3.

As it can be appreciated, all the measurements performed on the faces with outer skin show higher values of thermal conductivity than those found in measurements over surfaces without it (Table 2). This effect is due to the higher local density of the volume covered by the heat wave, which covers a lower probing depth for this smaller sensor. Regarding samples 5, it is also observed that the conductivity at the bottom face, in which there is a thick layer of metal, is much higher than that at the top face. Moreover, the results are sensitive to the presence of pores close to the skin under measurement (lower value in the *+Y* direction), as illustrated in Fig. 4 for sample 5-c. In the case of samples 2, thermal conductivity obtained in several directions presented no significant variations, and this is related to the homogeneous structure showed in CT

Table 3
Experimental values of thermal conductivity obtained in different directions in samples 5-a–c and 2-a–b

Direction	Thermal conductivity (W/m K)
Sample 5	
−Y	41.9
+Y	61
−Z	74
+Z	37.1
Sample 2	
−Y	31.0
+Y	29.9
−Z	33.7
+Z	30.8

images (Figs. 3 and 4). Nevertheless, even the slight asymmetries in the Z and Y profiles for sample 2 are also reflected in values of Table 3 with slightly lower values for $-Z$ and $-Y$ faces. These results are more evident in sample 5.

5.3. Theoretical models for thermal conductivity

Conduction through the solid phase, conduction through the gas phase, convection of the gas and radiation are the main mechanisms which may, at first, contribute to the thermal conductivity of a cellular material [31]. Taking into account previous works by Babcsán et al. [7] and Lu and Chen [9], only the conduction mechanism is considered in this work. In this section a brief revision of several theoretical models for the solid phase conduction is presented, comparing the predictions, after suitable theoretical simplifications, with the experimental results measured in X direction. A wide variety of models, all of them proposed for closed-cell foams, are considered in this work.

First of all, it is necessary to consider the simplest models: the Series–Parallel and the Parallel–Series models which both assume a cubical geometry. In the first, vertical cell walls and gas phase are combined in series to give a two-phase system. To obtain an expression for the whole material, horizontal cells walls are combined in parallel with the previous system [16]. In case of the Parallel–Series model first are combined the horizontal cell walls as depicted in Fig. 7. The final expressions for thermal conduction are

$$\text{Series—Parallel model}: \lambda_{gs} = \lambda_s(1 - V_g^{2/3}) + \frac{\lambda_s V_g^{2/3}}{\lambda_g + (\lambda_s - \lambda_g)V_g^{1/3}} \tag{5}$$

$$\text{Parallel—Series model}: \lambda_{gs} = \lambda_s \frac{\lambda_s - (\lambda_s - \lambda_g)V_g^{2/3}}{\lambda_s - (\lambda_s - \lambda_g)(V_g^{2/3} - V_g^{)}} \tag{6}$$

where λ_{gs} is the overall conductivity of the foam based on conduction through the combined gas and solid phase, λ_s and λ_g are the conductivities of the solid (aluminium) and gas phase (air), respectively, and V_g is the volume fraction of gas in the cellular material also named porosity. It is important to consider that these two models are a combination of the more basic parallel and series models which are not themselves realistic but predict maximum and minimum possible values for thermal conductivity in two-phase systems.

Doherty et al. modelled conduction trough two-dimensional squared bubbles which represents an advance in comparison to the previous ones. If extended to three dimensions the results of Doherty et al. agree with those of Russell [32].

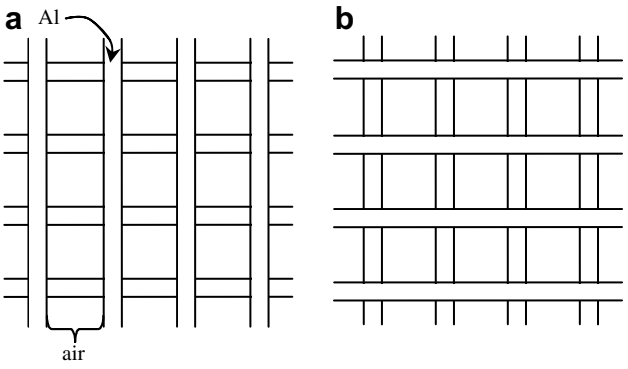

Fig. 7. Cubic cell foam models (a) Series–Parallel model and (b) Parallel–Series model.

$$\text{Doherty model}: \lambda_{gs} = \frac{\lambda_s\lambda_g(2V_g + 1) + 2\lambda_s^2(1 - V_g)}{\lambda_g(1 - V_g) + \lambda_s(2 + V_g)} \tag{7}$$

Russell [32] analysed conduction through a solid matrix with cubic cells arranged in-line. The cubic pores were assumed to have a uniform cell-wall thickness and struts were ignored. The next equation represents an upper limit result for an in-line cubic array of cells.

$$\text{Russell model}: \lambda_{gs} = \lambda_g\left(\frac{V_g^{2/3} + (\lambda_s/\lambda_g)(1 - V_g^{2/3})}{(1 - V_g^{2/3} + V_g) + (\lambda_g/\lambda_s)(V_g^{2/3} - V_g)}\right) \tag{8}$$

Other expression was suggested by Maxwell [15,32]. He assumed a polyphase composite in which spheres of one phase are randomly dispersed in a second phase (not in-line as in the Russell model). The final result of this model is

$$\text{Maxwell model}: \lambda_{gs} = \lambda_g\left(\frac{2V_g + 1 + \lambda_s/\lambda_g(2(1 - V_g))}{\lambda_s/\lambda_g(1 - V_g) + (2 + V_g)}\right) \tag{9}$$

For a material consisting of a solid skeleton with arbitrary air inclusions, it is possible to apply Misnar's model [8], in which heterogeneous bodies are considered as a mixture of a viscous phase with particles of a filler. In the theoretical considerations, fillers are supposed to have a regular geometric shape and the particles are assumed to be uniformly distributed throughout the entire volume. It this paper the authors estimate the upper limit for the model as

$$\text{Misnar model}: \lambda_{gs} = \lambda_s\left(1 + \frac{1 - \lambda_s/\lambda_g}{1 - V_g^{1/3}(1 - \lambda_s/\lambda_g)}\right) \tag{10}$$

An expression by Bruggemann for particles of various shapes dispersed in a continuous matrix reduces to Eq. (11) for the special case of spherical particles [15].

$$\text{Bruggemann model}: 1 - V_g = \left(\frac{\lambda_g - \lambda_{gs}}{\lambda_g - \lambda_s}\right)\left(\frac{\lambda_s}{\lambda_{gs}}\right)^{1/3} \tag{11}$$

Other interesting expression to be analysed is the Eucken model, also revised by Collishaw [15]

$$\text{Eucken model}: \lambda_{gs} = \lambda_s\left(\frac{1 + 2V_g[(1 - (\lambda_s/\lambda_g))/(2(\lambda_s/\lambda_g) + 1)]}{1 - V_g[(1 - (\lambda_s/\lambda_g))/(2(\lambda_s/\lambda_g) + 1)]}\right) \tag{12}$$

Finally Ashby, based on Glicksman's theoretical assumptions proposed a theoretical model for closed-cell cellular materials [27]. The expression obtained by Glicksman is a lower limit – i.e. valid for very high porosities – . It is important to consider it because nowadays it is one of the most accepted models for the conduction mechanism in thermal conductivity. The expression proposed by Ashby is

$$\text{Ashby model}: \lambda_{gs} = \xi\lambda_s(\rho_f/\rho_s) = \xi\lambda_s(1 - V_g) \tag{13}$$

where ρ_f and ρ_s are foam and solid density, respectively, and ξ is an efficiency factor which allows for the tortuous shape of the cell walls, which ranges between 1/3 and 2/3.

Two more empirical models have been taken into account. Progelhof [33] presented an empirical correlation derived from experimental results based on thermal conductivity of polymeric foams, in which n is an experimental fitting parameter. Finally, a scaling relation is proposed for the metallic foams in the book "Metal foams a design guide" [34], n is a fitting parameter in this equation.

Table 4
Original and simplified models

Name	Model	Simplified model[a]
Series–Parallel	$\lambda_{gs} = \lambda_s(1 - V_g^{2/3}) + \frac{\lambda_s V_g^{2/3}}{\lambda_g + (\lambda_s - \lambda_g)V_g^{1/3}}$	$\lambda_{gs} = \lambda_s(1 - V_g^{2/3})$
Misnar	$\lambda_{gs} = \lambda_s\left(1 + \frac{1 - \lambda_s/\lambda_g}{1 - V_g^{1/3}(1 - \lambda_s/\lambda_g)}\right)$	$\lambda_{gs} = \lambda_s(1 - V_g^{2/3})$
Parallel–Series	$\lambda_{gs} = \lambda_s \frac{\lambda_s - (\lambda_s - \lambda_g)V_g^{2/3}}{\lambda_s - (\lambda_s - \lambda_g)(V_g^{2/3} - V_g)}$	$\lambda_{gs} = \lambda_s \frac{1 - V_g^{2/3}}{1 - (V_g^{2/3} - V_g)}$
Russel	$\lambda_{gs} = \lambda_g\left(\frac{V_g^{2/3} + (\lambda_s/\lambda_g)(1 - V_g^{2/3})}{(1 - V_g^{2/3+V_g}) + (\lambda_g/\lambda_s)(V_g^{2/3} - V_g)}\right)$	$\lambda_{gs} = \lambda_s \frac{1 - V_g^{2/3}}{1 - (V_g^{2/3} - V_g)}$
Maxwell	$\lambda_{gs} = \lambda_g\left(\frac{2V_g + 1 + \lambda_s/\lambda_g(2(1 - V_g))}{\lambda_s/\lambda_g(1 - V_g) + (2 + V_g)}\right)$	$\lambda_{gs} = \lambda_s\left(\frac{2 \cdot (1 - V_g)}{(2 + V_g)}\right)$
Doherty	$\lambda_{gs} = \frac{\lambda_s\lambda_g(2V_g + 1) + 2\lambda_s^2(1 - V_g)}{\lambda_g(1 - V_g) + \lambda_s(2 + V_g)}$	$\lambda_{gs} = \lambda_s\left(\frac{2 \cdot (1 - V_g)}{(2 + V_g)}\right)$
Eucken	$\lambda_{gs} = \lambda_s\left(\frac{1 + 2V_g[(1 - (\lambda_s/\lambda_g))/(2(\lambda_s/\lambda_g) + 1)]}{1 - V_g[(1 - (\lambda_s/\lambda_g))/(2(\lambda_s/\lambda_g) + 1)]}\right)$	$\lambda_{gs} = \lambda_s\left(\frac{2 \cdot (1 - V_g)}{(2 + V_g)}\right)$
Bruggemann	$1 - V_g = \left(\frac{\lambda_g - \lambda_{gs}}{\lambda_g - \lambda_s}\right)\left(\frac{\lambda_s}{\lambda_{gs}}\right)^{1/3}$	$\lambda_{gs} = \lambda_s(1 - V_g)^{3/2}$
Progelhoff	$\lambda_{gs} = \lambda_g(1 + \lambda_s/\lambda_g \cdot (\rho_f/\rho_s)^n)$	$\lambda_{gs} = \lambda_s(1 - V_g)^n$
Scaling relationship	$\lambda_{gs} = \lambda_s \cdot (\rho_f/\rho_s)^n = \lambda_s \cdot (1 - V_g)^n/n \in [1.65, 1.85]$	$\lambda_{gs} = \lambda_s(1 - V_g)^n$
Ashby (Glicksmann)	$\lambda_{gs} = \xi\lambda_s(\rho_f/\rho_s) = \xi\lambda_s(1 - V_g)$	$\lambda_{gs} = \xi\lambda_s(1 - V_g)$

[a] Simplification for Misnar's model have been taken from the Ref. [9]. In some cases it has been also considered the low value of Vg compared to other terms.

$$\text{Progelhof model}: \lambda_{gs} = \lambda_g(1 + \lambda_s/\lambda_g \cdot (\rho_f/\rho_s)^n) \quad (14)$$

$$\text{Scaling relation } \lambda_{gs} = \lambda_s \cdot (\rho_f/\rho_s)^n = \lambda_s \cdot (1 - V_g)^n/n \in [1.65, 1.85] \quad (15)$$

Table 4 shows all the models. In the last column the models are compared and simplified using the assumption $\lambda_s \gg \lambda_g$. From the initial 11 models summarized in this paper it is possible to check that only five models give different equations as a function of porosity, V_g.

The simplified models are plotted in Fig. 8 together with the experimental data. The labels for the different theoretical models are those of the first equation for each group (Table 4).

The experimental parameter found according to Progelhoff's model and the Scaling relation was 1.55 ± 0.02. An experimental value of 0.57 ± 0.02 was found for the tortuosity parameter within Ashby's model.

Fig. 8 shows the mismatch between the experimental data and the Parallel–Series, Series–Parallel and Maxwell models. All these models overestimate the thermal conductivity, especially for high-porosity foams. On the other hand, Ashby's model fits acceptably for high porosity but, as the Glicksman's model assumes the lower limit important differences exist for the range of lower porosities. The best fit is obtained using the Bruggemann's model, with an exponent of 3/2 = 1.5 which is very near to the fitted exponent obtained from the experimental data (1.55). A slight disagreement in comparison with the exponent proposed for the scaling relation

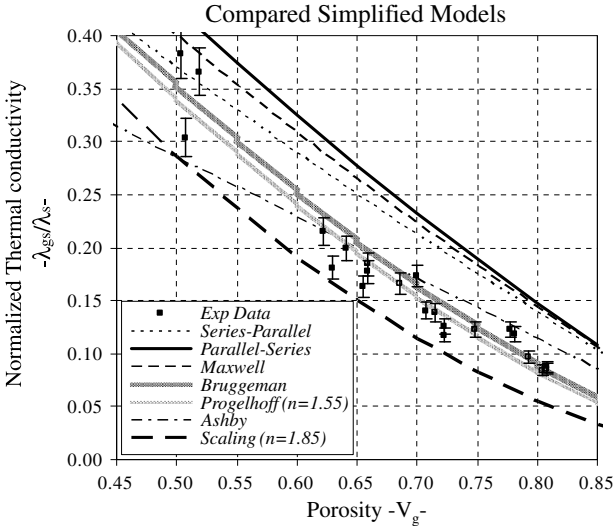

Fig. 8. Simplified models predictions as a function of the foam porosity compared to experimental data. λ_s was taken 167 W/m K.

(n = 1.65–1.85) is obtained. In the figure the data for maximum possible exponent (1.85) for this model are also presented. The predicted values are in this case lower than the experimental data.

A possible explanation for the differences between experimental results and predictions at high porosities of some of the models is related to the defects of the cellular structure. As described by Lu and Chen, the apparent thermal conductivity of the foam depends upon the cell shape, connectivity and topology, and it decreases in the presence of one of the several different types of geometrical imperfections: Plateau borders, fractured cell walls, missing cells, cell-wall misalignments, cell size variations and solid inclusions. The knock-down effect is more pronounced if several types of imperfection coexist in the cellular structure [9]. As theoretical models do not assume geometrical imperfections, it is logical to think that thermal properties for aluminium foams are lower than those expected theoretically. Specifically, low-density aluminium foams present a higher number of defects and for this reason most of the models overestimate the conductivity in the range of high porosities.

Finally, regarding Ashby's model it is important to report the possibility of modelling a porosity-dependent tortuosity, moreover this factor can be corrected by the fraction of solid in the struts (f_s) within Glicksman theory [32] according to

$$\xi = \frac{1}{3}(2 - f_s) \tag{16}$$

It could be possible to perform these calculations by measuring or modelling the dependency $f_s = f_s\ (V_g)$, although it would be only applicable for low-density metallic foams with porosities over 0.8.

6. Conclusions

The transient plane source method seems to be a powerful tool to measure and analyse several aspects related to the thermal conductivity of metallic foams. Using this method it has been possible to reach the following conclusions for a collection of AlSi7 foams produced via the powder metallurgical route:

- Measurements on the cut faces (X axis) were carried out, showing a power-trend decrease with the increasing porosity for the complete range of samples. The in-homogeneity in samples did not affect values in X direction because of a nearly constant density along that axis. Results in this work are in the same trend that values obtained by other authors.
- The CT results showed a high in-homogeneity in the Y and Z directions with independence of the sample's characteristics. The non-symmetric density profiles are related to the presence of drainage at the bottom part for the Z direction and to the presence of big pores for the Y direction.
- By means of the TPS technique it is possible to detect in-homogeneities in the samples, such as the non-uniform skin thickness or large pores as shown in measurements for Y and Z directions.
- The TPS technique may develop into a competitor for the traditional non-destructive techniques used in aluminium foams, with a lower equipment cost and lower measurement times. An envisaged quality control system based on the TPS technique would use several measuring heads in a part-dependent configuration which could easily be re-positioned to suit other geometries. Especially small and medium scale production could profit from this flexibility, while reduced times of analysis would benefit any production scenario.

A revision of theoretical models was performed. After suitable approximations initial models were reduced to only five. Comparing theoretical predictions with experimental results, classical models (Series–Parallel, Parallel–Series and Maxwell type) did not present good fittings. Only models with an adjustable experimental parameter and the Bruggemann's model, showed the best agreement with thermal conductivity values. Finally, Ashby's model seemed to fit only in the high porosities range. The effect of defects of the cellular structure could be one of the main sources for the differences between experimental results and some of the models predictions.

Acknowledgements

Financial assistance from CICYT (MAT 2002-04505-C02-01, MAT 2003-0697 and MAT 2006-11614-C03-01) and FEDER funding are gratefully acknowledged. Additionally the authors are grateful to the Spanish Ministry of Science and Education which supported this work with a FPU Grant Ref-AP-2004-2908 given to Mr. Solórzano.

References

[1] J. Banhart, Manufacture, characterization and application of cellular metals and metal foams, Prog. Mater. Sci. 46 (2001) 559–632.
[2] G. Evans, J.W. Hutchinson, M.F. Ashby, Cellular metals, Solid State Mater. Sci. 3 (1998) 288–303.
[3] J. Banhart, M.F. Ashby, N.A. Fleck, Adv. Eng. Mater. Met. 4 (10) (2002) 781–785.
[4] V.V. Calmidi, R.L. Mahajan, The effective thermal conductivity of high porosity fibrous metal foams, J. Heat Transfer 121 (1999) 466–471.
[5] A. Bhattacharya, V.V. Calmidi, R.L. Mahajan, Thermophysical properties of high porosity metal foams, Int. J. Heat Mass Transfer 45 (2002) 1017–1031.
[6] K. Boomsma, D. Poulikakos, On the effective thermal conductivity of a three dimensionally structured fluid-saturated metal foam, Int. J. Heat Mass Transfer 44 (2001) 827–836.
[7] N. Babcsán, I. Mészáros, N. Herman, Thermal and electrical conductivity measurements on aluminium foams, Materialwiss. Werkstofftech. 34 (2003) 391–394.
[8] A.N. Abramenko, A.S. Kalinichenko, Y. Burtser, V.A. Kalinichenko, S.A. Tanaeva, I.P. Vasilenko, Determination of the thermal conductivity of foam aluminum, J. Eng. Phys. Thermophys. 72 (3) (1999) 369–373.
[9] T.J. Lu, C. Chen, Thermal transport and fire retardance properties of cellular aluminium alloys, Acta Mater. 47 (5) (1999) 1469–1485.
[10] T.J. Lu, H.A. Stone, M.F. Ashby, Heat transfer in open-cell metal foams, Acta Mater. 46 (10) (1998) 3619–3635.
[11] J.W. Paek, B.H. Kang, S.Y. Kim, J.M. Hyun, Effective thermal conductivity and permeability of aluminum foam materials, Int. J. Thermophys. 21 (2) (2000) 453–464.
[12] V.V. Calmidi, R.J. Mahajan, Forced convection in high porosity metal foams, J. Heat Transfer 122 (2000) 557–565.
[13] S.Y. Kim, B.H. Kang, J.H. Kim, Forced convection from aluminium foam materials in an asymmetrically heated channel, Int. J. Heat Mass Transfer 44 (2001) 1451–1454.
[14] M.S. Phanikumar, R.L. Mahajan, Non-darcy natural convection in high porosity metal foam, Int. J. Heat Mass Transfer 45 (2002) 781–3793.
[15] P.G. Collishaw, J.R.G. Evans, An assessment of expressions for the apparent thermal conductivity of cellular materials, J. Mater. Sci. 29 (1994) 486–498.
[16] A.G. Leach, The thermal conductivity of foams. I. Models for heat conduction, J. Phys. D: Appl. Phys. 26 (1993) 733–739.
[17] T. Sakiyame, Y. Matsushisa, Y. Shiinoki, T. Yano, Finite-element analysis on the effective thermal conductivity of dispersed systems of spheres of various sizes, J. Food Eng. 11 (1990) 317–331.
[18] Y. Xu, K. Yagi, Automatic FEM model generation for evaluating thermal conductivity of composite with random materials arrangement, Comput. Mater. Sci. 30 (2004) 242–250.
[19] I.V. belova, G.E. Murch, Monte Carlo simulation of the effective thermal conductivity in two-phase material, J. Mater. Process. Technol. 153–154 (2004) 741–745.
[20] F. Baumgärtner, I. Duarte, J. Banhart, Industrialization of powder compact foaming, Adv. Eng. Mater. 2 (4) (2000) 168–174.
[21] V. Gergely, B. Clyne, The formgrip process: foaming of reinforced metals by gas release in precursors, Adv. Eng. Mater. 2 (4) (2000) 175–178.
[22] E. Maire, L. Babout, J.Y. Buffiere, R. Fougeres, Recent results on 3D characterization and damage of metal matrix composites and a metallic foam using X-ray tomography, Mater. Sci. Eng. A319–321 (2001) 216–219.
[23] O.B. Olurin, M. Arnold, C. Körner, R.F. Singer, The investigation of morphometric parameters of aluminium foams using micro-computed tomography, Mater. Sci. Eng. A328 (2002) 334–343.
[24] J. Banhart, D. Bellmann, H. Clemens, Investigation of metal foam formation by microscopy and ultra small-angle neutron scattering, Acta Mater. 49 (2001) 3409–3420.
[25] T. Log, S.E. Gustafsson, Transient Plane Source (TPS) technique for measuring thermal transport properties of building materials, Fire Mater. 19 (1995) 39–43.
[26] M. Gustavsson, E. Karawacki, S.E. Gustafsson, Thermal conductivity, thermal diffusivity and specific heat of thin samples from transient measurements with hot-disk sensors, Rev. Sci. Instrum. 65 (1994) 3856–3859.

[27] S.E. Gustafsson, Transient Plane Source (TPS) technique for thermal conductivity and thermal diffusivity measurements of solid materials, Rev. Sci. Instrum. 62 (1991) 797–804.
[28] V. Singhal, P.J. Litke, A.F. Black, S.V. Garimella, An experimentally validated thermo-mechanical model for the prediction of thermal contact conductance, Int. J. Heat Mass Transfer 48 (2005) 5446–5459.
[29] E.G. Wolff, D.A. Schneider, Prediction of thermal contact resistance between polished surfaces, Int. J. Heat Mass Transfer 41 (1998) 3469–3482.
[30] <www.matweb.com>.
[31] L.J. Gibson, M.F. Ashby, Cellular Solids, second ed., Cambridge University Press, Cambridge, 1997.
[32] L.R. Glicksman, Heat transfer in foams, in: N.C. Hilyard, A. Cunningham (Eds.), Low Density Cellular Plastics – Physical Basis of Behaviour, Chapman and Hall, London, 1994, pp. 107–111.
[33] R.C. Progelhof, J.L. Throne, Cooling of structural foams, J. Cell. Plast. 11 (1975) 152–163.
[34] M.F. Ashby, A.G. Evans, N.A. Fleck, L.J. Gibson, J.W. Hutchinson, H.N.G. Wadley, Metal foams: A Design Guide, Butterworth Heinemann, Oxford, 2000.